MED-Vol. 2-1
MH-Vol. 3-1

MANUFACTURING SCIENCE AND ENGINEERING – 1995 VOLUME 1

- MATERIAL REMOVAL AND SURFACE MODIFICATION ISSUES IN MACHINING PROCESSES
- MECHATRONICS FOR MANUFACTURING
- COMPUTER-AIDED TOOLING

presented at
THE 1995 ASME INTERNATIONAL
MECHANICAL ENGINEERING CONGRESS AND EXPOSITION
NOVEMBER 12–17, 1995
SAN FRANCISCO, CALIFORNIA

sponsored by
THE MANUFACTURING ENGINEERING DIVISION, ASME
THE MATERIALS HANDLING DIVISION, ASME

principal editor
ELIJAH KANNATEY-ASIBU, JR.
UNIVERSITY OF MICHIGAN, ANN ARBOR

contributing editors
C. JAMES LI
RENSSELAER POLYTECHNIC INSTITUTE

YIMING (KEVIN) RONG
SOUTHERN ILLINOIS UNIVERSITY, CARBONDALE

CHIH-YUAN SHIA
ADVANCE MILWAUKEE BRUSH MFG. CO.

ROBERT J. STANGO
MARQUETTE UNIVERSITY

THE AMERICAN SOCIETY OF MECHANICAL ENGINEERS
UNITED ENGINEERING CENTER / 345 EAST 47TH STREET / NEW YORK, N.Y. 10017

MED-Vol. 2-1/MH-Vol. 3-1, Manufacturing Science and Engineering
ASME 1995

MODEL-BASED QUALITY OPTIMISATION FOR LASER CUTTING UNDER TRANSIENT CONDITIONS

P. Di Pietro, A. Jeromin
School of Mechanical and Manufacturing Engineering
The University of New South Wales
Kensington, New South Wales
Australia

Y. L. Yao
Department of Mechanical Engineering
Columbia University
New York

ABSTRACT

Quality improvements in laser cutting of mild steel have been achieved by a newly developed model-based optimisation strategy. The specific aims of such efforts are to assure quality of cut right up to pre-cut sections and boundaries, which are inherent in intricate part programs. Such boundaries frustrate heat transfer and result in bulk heating of the workpiece. This in turn leads to a degradation of the cut quality. In order to focus on the development of such optimisation, constant thermo-physical properties and two-dimensional transient heat conduction is simply assumed. The model is therefore valid for the thin plate laser cutting case, where temperatures are approximately homogeneous with workpiece depth. Close inspection of the laser-workpiece interaction zone reveals that the cutting front exhibits dynamic behaviour, and such mobility plays a significant role in temperature determination. Non-linear parameter adaption profiles are generated via the optimisation strategy in order to stabilise cutting front temperatures. Currently, extensive trial-and-error based experimentation is needed in order to improve cut quality in such regions. Thus model-based optimisation has the added benefit of reducing this time-exhaustive step whilst leading to an optimal solution. Experimental results are presented and it is demonstrated that such process manipulation can lead to significant quality improvements.

NOMENCLATURE

amu	atomic mass units
b	kerf width
Bi	mesh-size biot number
c_v	heat capacity
D	workpiece thickness
H	net energy input
h_f	forced convective heat transfer coefficient
h_n	natural or free convective heat transfer coefficient

h_r	radiative heat transfer coefficient
I(r)	radial intensity distribution
I(0)	peak intensity
K	thermal conductivity
k	proportionality constant
L	workpiece length
L_f	latent heat of fusion
$\dot{m}$	melt removal rate
$P_b(r)$	radial absorbed beam power
P_{exo}	exothermic power
P_{inc}	incident beam power
P_{melt}	melting power
P_{trans}	transmitted power
$\dot{q}$	heat generation
r	radial distance from beam centre
ratio	ratio of FeO:Fe
R_b	laser beam radius
S	molten layer thickness
T	temperature
T_{melt}	melting temperature
t	time
V_b	velocity of laser beam
V_f	velocity of cutting front
W	workpiece width
x, y, z	co-ordinate axes
Y_b	laser beam position
Y_d	initial drilling position

Superscripts and subscripts

f	front location
j	current time
m	nodal point in y direction
n	nodal point in x direction
∞	ambient conditions

Greek letters

α	thermal diffusivity
ΔH	exothermic energy release
ΔP	incremental power level
ΔS	change in molten layer thickness from previous location
ΔS_b	distance beam has moved from its previous location
ΔS_f	distance front has moved from its previous location
Δt	timestep of integration
ΔT	temperature tolerance
$\Delta y = \Delta x$	spatial increments
σ	mesh fourier number
ρ	density

INTRODUCTION

Today, laser cutting of highly complex and intricate workpieces is a reality. Of concern though, is the effect of part geometry on the quality achievable. Such part programs typically contain many pre-cut sections and boundaries, and because of the obvious size of such workpieces, heat accumulation is often severe. This can result in

poor cutting quality in the form of widespread burning, increased dross, increased surface roughness and kerf widening being common amongst other problems. The appearance of even one of these anomalities can render the complete job useless.

In cases where heat fluxes are strong enough to melt the material as in laser cutting, the problem becomes complex due to the moving solid-liquid interface. Efficient cutting occurs when the beam rides ahead on the unmolten material and therefore little energy falls through the generated cut. When the cutting front speed increases due to heat accumulation, or when cutting at slow processing speeds, the beam tends to lag behind the front. As a result, much more laser beam energy passes through the cut with little or no heating effect. Such characteristics of the process alter the amount of energy input into the interaction zone, and therefore cutting front temperatures are expected to change. Consequently, such temperature deviations are attributable to the generation of inconsistent cut quality.

There have been many models developed over the years to describe the laser cutting process. A comprehensive review of these is given elsewhere by the authors Di Pietro and Yao (1994). In particular, Gonsalves and Duley (1972) first accounted for the fact that only part of the incident beam power is available for laser cutting sheet metals. This fraction was determined using a moving point source model. The model was used to determine the interrelationship between cutting speed, cut width and power required for efficient laser cutting. Powell (1993a) devised cutting experiments to investigate the transmission and reflection losses occurring in the cutting process based on previous work done by Miyamoto, Maruo and Arata (1984, 1986). It was shown that the amount of reflected/transmitted light reduced as sample thickness was increased. Schreiner-Mohr, Dausinger, and Hugel (1991) also conducted experimental work which showed that at maximum cutting speeds, the beam centre can precede the front location. At slow cutting speeds the beam centre was shown to lag behind the cutting front. A mono-dimensional finite difference model was proposed by Yuan, Querry, and Bedrin (1988) which suggested that the cutting front could possess mobility when cutting at constant processing speeds. Arata et al. (1979) showed through high speed photography that the cutting front was indeed dynamic in nature, and the formation of striations on the kerf walls could be explained well by the relative movement between the front and the laser beam.

Previous attempts at characterising the process have often assumed infinite workpiece length or they have prescribed fixed boundary temperatures. But in laser cutting of intricate parts, this assumption leads to low heat accumulation estimates. Such simplifications allow the general heat conduction equation to revert to the case of steady multi-dimensional conduction. A transient model is therefore developed to account for workpiece geometry and the presence of a kerf is considered, with nodal points within it becoming part of the convective environment. Thin plate laser cutting is considered, so that the model can assume the two-dimensional heat conduction form in order to reduce the complexity of the optimisation tasks. Inherent problems associated with a moving cutting front and temporal variations of the energy input per unit time are resolved (including not only transience in the absorbed beam power because of coupling issues but also in the exothermic reaction energy). These issues require a numerical approach, which would otherwise be impossible to address analytically.

MATHEMATICAL FORMULATION

A complete description of the mathematical formulation has been presented elsewhere by the authors, Di Pietro and Yao (1995). A summary is given below. Fig. 1 shows a schematic of the laser cutting process. If we assume constant thermo-physical properties and the temperature distribution is homogeneous along the depth of the workpiece ($\partial T/\partial z=0$, as can be assumed for the thin plate laser cutting case) then this reduces to the simpler two-dimensional transient heat conduction equation. This criterion implies that the temperature at the upper workpiece surface approximates the lower surface temperature at every point in the control volume.

$$\frac{K}{\rho c_v}\left(\frac{\partial^2 T}{\partial x^2}+\frac{\partial^2 T}{\partial y^2}\right)+\frac{\dot{q}}{\rho c_v}=\frac{\partial T}{\partial t} \qquad (1)$$

The laser beam initially heats up and melts the material directly beneath it. The pressure from the oxygen supply through the cutting nozzle then blows the molten material away. A cut is generated therefore as the beam traverses across the workpiece. Forced convection from the gas provides some cooling to this region, but its contribution is greatly outweighed by the exothermic reaction that is produced between the oxygen and the molten material. Fully developed turbulent flow is assumed for the forced convection case, although turbulence within the kerf can somewhat be minimised by adjusting the nozzle-standoff distance.

The material removal process is in actual fact a rather complex interaction of the gas jet on the free surface of the melt, where shear stresses act on the cutting front and a boundary layer exists. It is assumed in our model that any area in the molten state is expelled out of the kerf immediately, by the force of the gas jet.

At all points other than where the oxygen gas jet impinges, it is assumed that there is no farfield streaming and thus natural or free convection occurs. Although its contribution is relatively small, it too is included for the sake of completeness. Heat transfer to the substrate can also be an important factor but we have assumed the use of a nail bed, honeycomb or mesh support, thus their conductive effect is small. Some minor reflections may occur in practice though, from the beam striking the substrate and deflecting it back into the kerf.

Let us assume that the CO_2 laser source is of Gaussian TEM_{oo} mode. Its radial intensity distribution can then be given as

$$I(r) = I(0)\ \exp\left(-2r^2 / R_b^2\right), \qquad (2)$$

where R_b is the laser beam radius at which point the power distribution falls to the industry accepted $1/e^2$ level.

Of the energy arriving at the cutting front, only a small percentage is absorbed. This is especially true when we consider depolarised or circularly polarised laser beams as is the case with co-ordinated motion laser cutting systems. Absorptivity values can be as low as 0.1, which is often limited by the oxide layer surface absorptivity about the cut face.

The energy produced by the exothermic reaction cannot be neglected as its contribution is generally of the same order of magnitude as the absorbed laser beam power. It has been shown by Powell et al. (1992, 1993b) (through an ejected particle analysis) that approximately 50% of the melt ejected from the kerf is Fe and the remainder is almost completely FeO. Assuming a pure oxygen supply for the assist gas, the following reaction occurs within the cutting kerf

$$Fe + 0.5\ O_2 = FeO \qquad \Delta H = -257.58\ \text{kJ/mol},$$

where ΔH is the energy released during the reaction. Geiger, Bergmann, and Nuss (1988) determined that the ignition point for the burning of steel with oxygen is approximately 1473.15K.

If the mass removal rate of the melt out of the kerf is known or can be calculated, then the following relationship can be used to determine the energy obtained by reaction.

$$P_{exo} = \text{ratio}\left(\frac{\dot{m}\,\Delta H}{\text{amu}}\right) \qquad (3)$$

where amu = 1 mole FeO = 71.847 g/mol and ratio is the percentage of FeO:Fe ejected from the kerf.

This ratio is extremely sensitive to gas impurity levels, and the diffusion rate of O_2 into the melt is increased with increasing gas pressure. These factors make the prediction of this term difficult to establish in practice, whilst pressure variations are also common during cutting.

Because the material within the kerf is melted and then expelled out, it is necessary to consider latent heat effects. In laser welding this is often neglected because the latent heat of fusion is compensated by the latent heat of solidification. In cutting though, the material is removed and as such, only a very small liquid layer along the walls of the kerf can contribute to this heat of solidification.

$$P_{melt} = \dot{m} L_f \qquad (4)$$

where $L_f = 275$ kJ/kg.

The cutting front speed is an important factor affecting the mass removal rate. Under steady state conditions this speed approaches the cutting speed, but under a boundary encroachment, these values can differ greatly. The mass removal rate is therefore more appropriately given as

$$\dot{m} = \rho b D V_f \qquad (5)$$

V_f physically represents the solid-liquid interface speed, as all the molten material is assumed to be ejected out of the bottom of the kerf immediately. If the beam speed is too high, then melting and evaporation will cease. In this case, no melt ejection is possible and Eqn. (5) becomes invalid. This condition is continually checked throughout program execution and simulation ceases if it is violated.

Because kerf width fluctuations are generally small for high quality cutting, it is assumed that they are negligible and that the width is approximately of the same extent as that of the laser spot diameter. The kerf is therefore assumed to have a rectangular cross-section and the cutting front is assumed to be vertical.

An Optimisation Strategy via Power Control

The Japanese corporation Mitsubishi (Moriyasu et al., 1986), and other research groups realised early on that adaptive control of laser parameters was a real possibility with conventional CNC (computer numeric control) systems. By adapting parameters such as laser power levels, switching between continuous wave (CW) and pulsed mode, and effecting cutting speed changes, vast quality improvements were obtainable. Such techniques are trial-and-error based, and therefore are time consuming, whereby the optimal set of parameters may still not be reached. It was recognised by Biermann and Geiger (1991) that simulation of the laser process under the effects of the motion system can lead to improved results for laser processing.

An optimisation strategy is therefore proposed in which it forces the cutting front temperature to remain steady right up to a prescribed boundary. The problem of minimising the deviation from steady state results in a non-linear power profile, as the inter-relationships between laser parameters are complicated by the mobility exhibited by the cutting front. Uniform cutting front temperatures affect quality in various ways. They produce better quality by i) maintaining kerf widths more consistently, ii) producing more uniform heat-affected zones, and iii) reducing the amount of wide

spread self-burning. At the very least, uniform cutting front temperatures reduce the variability in cut quality which increases the odds that the final workpiece will reach acceptability standards.

The strategy developed is iterative by nature. Refer to Fig. 2. The model proceeds forward in time by the accumulation of the timestep Δt of integration. By monitoring the status of the front temperature at every instance, a steady state value can be established.

$$| T_f^{j+1} - T_f^j | < \Delta T \tag{6}$$

The cutting front temperature can only be disturbed subsequently by a boundary encroachment or by a speed change of the motion system. As the change in temperature exceeds the previously set limit ΔT, a course of action is required in the form of a power reduction of size ΔP.

$$\Delta P = | T_f^{j+1} - T_f^j | \times k \tag{7}$$

$$P_{inc}^j = P_{inc}^j - \Delta P \tag{8}$$

Eqn. (8) determines the size of the power reduction based on two pieces of information forwarded to the optimisation module. The larger the temperature rise, the larger is the reduction in laser beam power in order to return the system to its controlled state. This is achieved by the proportionality constant k, which effects the convergence rate of solution. Of course, if the constant is too large, then the temperature cannot be stabilised within the ΔT control limit.

COMPUTATIONAL METHODS

The determination of the mass removal rate is dependent upon firstly evaluating the cutting front speed. From Fig. 3, it can be shown that

$$\Delta S_f = \Delta S_b - S + (S + \Delta S) = \Delta S_b + \Delta S \tag{9}$$

In the time interval Δt, an expression for the front velocity can be ascertained.

$$\frac{\Delta S_f}{\Delta t} = \frac{\Delta S_b}{\Delta t} + \frac{\Delta S}{\Delta t} \tag{10}$$

The limit as $\Delta t \to 0$, yields the following instantaneous rates of change

$$\frac{\partial S_f}{\partial t} = \frac{\partial S_b}{\partial t} + \frac{\partial S}{\partial t} \tag{11}$$

From which Eqn. (11) can be expressed in the general form

$$V_f = V_b + \frac{\partial S}{\partial t} \tag{12}$$

where $\frac{\partial S}{\partial t}$ is the time rate of change of the molten layer thickness.

The molten layer thickness is given by the shortest distance from the melting isotherm to the laser beam's centre at any given time t. The melting isotherm then represents the solid-liquid interface. A numerical expression for the average time rate of change of the molten layer thickness over the interval Δt can be obtained for

evaluating the front velocity. This is done by using a method of first order interpolation between the nodal temperature T_m and the forward-shifted temperature T_{m+1}.

At time t = j

$$S^j = \Delta y \frac{(T_m^j - T_{melt})}{(T_m^j - T_{m+1}^j)} \tag{13}$$

where m denotes the nodal point of interest in the y direction. By analogy, at time $t+\Delta t = j+1$

$$S^{j+1} = \Delta y \frac{(T_m^{j+1} - T_{melt})}{(T_m^{j+1} - T_{m+1}^{j+1})} \tag{14}$$

from which

$$\frac{\Delta S}{\Delta t} = \frac{(S^{j+1} - S^j)}{\Delta t} \tag{15}$$

The percentage of power incident on the workpiece is therefore given by the proportion the cutting front is ahead of the trailing edge of the laser beam. Refer to Fig. 4. If the front is behind the trailing edge of the laser beam, then all the beam power will fall on the workpiece. This represents the most efficient beam coupling theoretically possible. In reality though, some beam leakage will always occur.

Numerical Issues

Table 1 summarises the model parameters used in the simulation and the thermo-physical properties assumed for mild steel. After material is expelled from the kerf, conduction cannot occur across this region as these points are now part of the convective environment. The model accounts for this by removing all nodes above melting point which fall within the extent of the assist gas stream.

Heat diffusion equations are determined for all nodal points within the control volume and at boundaries. These balance equations can be solved in a number of ways. Implicit formulations were chosen because they have unlimited numerical stability. All nodes were swept by their appropriate equations until the temperatures converged to some previously set limit (refer to the Appendix).

On most occasions, it is necessary to initiate a keyhole in the work material prior to cutting. This issue is considered so that a realistic cutting process is simulated. Molten material can only be ejected upwards in all directions until complete penetration. The model can be used to obtain minimum penetration times required to create such initiation holes, but to obtain more accurate penetration times, it is necessary to consider the formation of surface plasma (Yilbas et al., 1990). Once a kerf is formed, the effect of these plasma's are reduced somewhat due to the ability of the gas jet to remove them more effectively. Surface plasma's are neglected in this model as the main emphasis is to simulate the cutting process as opposed to the drilling one.

Once all the discretized equations have converged, the model determines the current front velocity, from which the exothermic power can be calculated. The percentage of transmitted power lost through the kerf is then evaluated. The status of the current laser beam position relative to the workpiece is updated and a new timestep of integration is obtained. The model then loops and the procedure is repeated until the laser beam reaches its user-specified final stopping position, or until front temperatures fall below melting point. This indicates that cutting conditions are poor and that quality can no longer be assured.

EXPERIMENTAL PROCEDURE

Experimental Setup

The experiments were performed on a fast axial flow 1.5 kW CO_2 laser (PRC model FH 1501). The beam mode is essentially TEM_{00}, with all experiments performed under continuous wave (CW) operation. The laser beam was focussed down to 250 μm, through a 5" ZnSe high pressure meniscus lens. The throat diameter of the nozzle used was 1 mm, and a nozzle-standoff distance of 1mm was maintained. Assist gas pressures were kept constant at 2.7 bar throughout the experiments.

Cold rolled mild steel plates (AS 1595) of 1 mm thickness, were guillotined into 20 mm square blanks. Cuts were initiated 5 mm in from one end, and cut down the centreline of the workpiece to the other end. All initiation keyholes were created by blast drilling with oxygen for a penetration period of 100 msec. Table 2 summarises the simulation and experimental conditions used.

In order to validate workpiece temperature distributions calculated to those determined experimentally, type K, chromel-alumel thermocouples were used. An overall diameter of 0.5 mm was chosen because thicker diameter thermocouples result in slower response times. The thermocouples were imbeded at various positions on the workpiece. These were chosen to avoid high temperature gradients closer to the line of cut and as such, allows the thermocouples to respond adequately. In addition, validation becomes difficult at very close positions to the line of cut because small shifts in thermocouple locations results in large variations. This is due to the large temperature gradients experienced around the interaction zone. The thermocouple positions were accurately checked using a microscope and data collection was triggered via an electrical relay in the controller which actuates the beam shutter mechanism.

Polymethylmethacrylate (PMMA) is the most important of the general class of acrylic polymers and goes under various trade names. PMMA has long been used in industry in qualitative visualisation for mode printing of laser beams and for alignment procedures. An experiment was setup, with the view of obtaining a better insight into the mechanism(s) affecting the reactive gas cutting of mild steel and for validation of transmitted power levels determined from the model.

Acrylic blocks (approx. 25 mm square, by 60 mm long) were placed 3 mm below the mild steel samples to obtain the burn prints. A strong air jet was used to remove the vapours produced, which if left unattended can ignite and destroy the prints left in the acrylic blocks.

A specific ablation energy (specific efficiency) of 3000 J/cm^3 for polymethylmethacrylate (PMMA) was established by Miyamoto, Maruo, and Arata (1984). Therefore by knowing the volume removed from the acrylic, together with the total time taken for the cut, power losses through the kerf can be ascertained. Cross-sectional profiles of the burn prints were carefully traced from photographic reproductions of the samples for visualisation of the mechanisms affecting the process.

High speed colour photography was also undertaken to examine and investigate cutting front mobility on approach to a workpiece boundary. Cine films were taken at a camera speed of 500 frames per second, and the camera (HITACHI - '16HM - HIMAC') was focussed directly on the laser-material interaction zone. It was positioned perpendicular to the line of cut at an angle of 15^0, so that any lateral movement of the front in the direction of cut could easily be discerned.

Analysis of the developed film was carried out under a Nikon Shadowgraph, so that large magnification of the front was possible. Mitutoyo digital micrometer heads facilitated accurate measurements of any movements observed.

Preparatory Work

Verifying Laser Beam Power Levels. In order to perform the experiments, actual power levels needed to be established for accurate model validation. A Macken P - 2000C power probe was subsequently used for this task. It is a calorimeter-type power meter, which measures unfocussed laser power using a timed exposure and relies on knowing the mass of material it heats up. Fig. 5 shows the power levels measured by the probe and its associated discharge current for one of eight discharges. Current control is via a 12 bit digital word which allows accurate manipulation through part programs generated.

Verifying Motion System Accelerations. It was shown previously by the authors, Di Pietro and Yao (1995) that the characteristics of the handling system affects the dynamics of the cutting front and as a result, will affect the quality of cut possible. All simulations therefore needed to be run under accelerations and decelerations which closely resembled those possible in practice. In order to achieve this, a TRANS-TEK 290 Series LVDT (AC-AC) was attached to the motion system. The axially displaced coil produces a change in voltage directly proportional to the displacement. After some amplification of the signal, it was fed into a data acquisition system.

Results showed that the CNC typically was capable of accelerating and decelerating at about 300mm/sec^2. This is in accordance with other commercially available systems. It should be noted that such motion profiles occur whilst under interpolation or contour mode, as opposed to point to point mode where no position error checking occurs.

RESULTS AND DISCUSSION

Comparing Workpiece Temperature Distributions

Often when computer processing of thermocouple data is needed, various n-th order polynomials are fitted to data. For precise analysis of the results, the thermocouples need to be calibrated directly against a known temperature source. In our case we have employed the use of an accurate industrial oven to provide the heating source.

The oven was set to reach 1000 ^{o}C over a period of one hour (NABER kiln with a microprocessor based temperature program controller - Model PS - 962C). The signal output was measured every 10 ^{o}C, with consistent, repeatable values only achievable up to an oven temperature of about 870 ^{o}C. After which, random voltage fluctuations were significant. Although the thermocouples can withstand such temperatures, the voltage output from the amplifier was somewhat limited. A reasonably linear relationship was observed between temperature and signal output, but actual data was used for signal analysis instead of a curve-fitting algorithm.

Fig. 6 shows typical results obtained from model execution as compared to experimentally determined values from the thermocouples. The thermocouples were imbeded 2 mm in from the corner of the workpiece closest to the initiation point in both the x and y directions. Different cutting speeds and power levels were validated, and the close correlations suggest that the thermocouples were able to respond fast enough.

Addressing Beam Coupling Issues

Fig. 7(a) shows the evaluation of total power losses obtained from the PMMA experiments at a constant laser power of 600 W. We can see that with speed increases, the amount of power lost through the kerf decreases. This indicates that the cutting process is more efficient at higher processing speeds, as the chance of more beam absorption is increased. Predicted power losses are also shown. They too show that losses are minimised at faster cutting rates, but the theoretical losses are

consistently less than the actual power losses experienced in practice. This is as expected as the model only determines the fraction of power loss resulting from light transmission directly through the kerf, and cannot account for the reflection mechanism. The discrepancies between the curves are therefore believed to be the result of the contribution of the reflected power to the overall burn print.

Fig. 8 shows the prints actually obtained from the PMMA samples. The cross-sectional profiles obtained give information about the mechanisms affecting the process. For example, Fig. 8(a) clearly shows interference fringe patterns, proof that the reflection mechanism exists in the laser cutting process. Interference patterns were observable up to 60 mm/sec, after which none could be clearly discerned. Such patterns are a direct result of laser light arriving at a distant point by two slightly different paths. Refer to Fig. 9. If the phase difference between the two waves is 2π, then this is equivalent to no phase difference and the waves will interfere constructively. The path difference will be exactly an integer times the wavelength of the laser light, which means the path difference can be as little as 10.6 μm to produce interference maxima. Fig. 8(d) interestingly shows that light reflection also occurred in the mode prints as a result of light piping or reflection off the steep sidewalls of the burn pattern. This is observable by the presence of a 'fish tail' at the initiation point.

If the extent of the contribution of such fringes is small, we can then assume that most of the losses are due to transmitted power passing directly through the kerf, but if large dominant fringes are observable, then we must conclude that a significant portion of these losses are transferred through the kerf via the reflection mechanism.

By subtracting the experimentally determined total power losses from the transmitted power values determined theoretically, an indication of the levels of reflection can be obtained. As the processing speed increases, the cutting front moves from a near vertical face to a sloping one. This results in less transmitted power being able to escape from the bottom of the cut, as more beam power can be absorbed further down the front. The theoretical results obtained support this generally accepted point. But one would presume that a steeper cutting front would result in greater reflection losses as more of the sloped face is exposed to the beam. Powell (1993a) gives an excellent explanation for why this is not the case. He suggests that at high cutting speeds, the cutting front becomes more curved at the bottom and traps the reflected light from further up the face. The shallow angle of the reflection results in a multiple reflection mechanism lower down and absorption is therefore more likely. Fig. 7(b) clearly shows that reflection is minimised with speed increases.

However Powell (1993a) mentioned that no interference patterns were observable when he conducted experiments on mild steel, but Fig. 8 shows their existence. Such phenomena were also observed at other power levels. It is believed that such maxima are dependent on the distance the PMMA print is obtained below the workpiece. This is because of the fact that the reflected and transmitted beams must be able to meet further down at a specific point in space. Changes in this distance may result in the beams having already interfered if placed too far below, or have not yet met if placed too close to the cut specimen.

Transient Effects on Boundary Encroachment

Fig. 10 shows the results obtained from a simulation when no control strategy was implemented and run at a power setting of 600 W and a processing speed of 20 mm/sec. Although the cutting speed remains constant right up to the workpiece edge, the front velocity begins to move on its approach to the boundary because heat diffusion is frustrated and over-heating of the area occurs. The increase in the front speed produces an increase in the exothermic power, but this increase in contrast, also results in more power falling through the kerf. The net effect of all these mechanisms working at once is best depicted by the increase in the cutting front temperature experienced by the boundary encroachment.

Visualisation of Cutting Front Mobility via High Speed Photography. High speed colour photography was undertaken in order to examine transient effects on approach to a boundary. Fig. 11 shows a portion of the film developed when cutting was carried out using the same parameters used in the simulation (ie. 600 W and 20 mm/sec). The final photograph of the front actually on the boundary is omitted because it was of poor quality, as self-burning of the workpiece occurred and resulted in a strong light emission which obscured the cutting front. It is clear though that as the cut proceeds closer to the prescribed boundary, the size of the melt increases and actually reaches a maximum value of 1.089 mm. Of more interest though is the fact that the cutting front speed also increased on approach to the workpiece edge. By measuring the relative distance moved by the front between frames and knowing the camera speed, an approximate measure of the cut speed could be determined. Refer to Fig. 12. Values were only evaluated over the final 0.3 mm because the periodic front motion ceased from this point onwards and so provided a clear picture of the dynamics in this region. Prior to this stage, the cyclic nature of the light emission tended to dominate the cutting mechanism and no gradual increase in the front speed was evident. Although some uncertainty lies in the absolute measurement of the front movement between frames, the trend is clear nevertheless.

Temperature Growth on Boundary Encroachment. The temperatures occurring in the vicinity of the interaction zone (especially when the laser beam reaches a boundary) are important because they affect the quality of cut considerably. Ideally, actual measurement of the cutting front temperature is preferred, but the harsh environment found under the nozzle (viz. space restrictions and high temperatures) makes this very difficult. Non-contact pyrometric measurements have been attempted by the authors, but absolute temperature values are not possible and the dependence on constant emissivity and slow response time amongst other factors led us to abandon this approach. Instead, thermocouple measurements were reverted to. These were imbeded 1.5 mm in from the prescribed boundary and 1.5 mm in from the intended line of cut. Again, closer positions to the interaction zone led to poor thermocouple response and small deviations in location produced erroneous results because of the large temperature gradients experienced about the interaction zone.

Fig. 13 shows typical transience experienced in practice on approach to a prescribed boundary as compared to numerical results. Again the cutting parameters used were 600 W and 20 mm/sec. Time histories of this temperature location are shown, and they can be seen to correlate well. As the beam approaches the boundary, conduction is frustrated and causes wide-spread bulk heat and accumulation, causing the temperatures in this region to soar. This is evident from both the experimental and numerical results. Such large transient effects at this position only highlights the fact that the actual cutting front must experience even more severe transience under the same conditions.

Power Manipulation for Quality Improvements

Fig. 14 shows the power profile determined by the model-based optimisation strategy for temperature stabilisation when cutting with 600 W at 20 mm/sec. In order to achieve actual quality improvements through this optimisation strategy, it is necessary to have current control or power control on the laser which can respond fast enough to closely approximate the theoretical profile. Tests were therefore performed to check the performance of the laser under rapidly changing commands.

Fig. 15 shows the response of a resonator discharge to a step input. A power change from zero to 1000 Watts was commanded via the controller. The signal was obtained from a BNC bulkhead receptacle located on the discharge current meter (mA). The output approximates a step response of a first-order system, and thus the time constant of the system was evaluated. It was found that the response reached 63.2 % of its total change in as little as 1.3 msec. After two time constants, the response had all but

reached its final value. Thus the laser control facility was adequate to perform the optimisation power strategies discussed.

First results are presented from the power adaption strategy. Fig. 16 shows photographs taken of the kerf produced with and without power control for the conditions mentioned above (ie. 600W and 20 mm/sec). Another typical example is also shown when run under different cutting conditions (ie. 800 W and 30 mm/sec). It is clear from the photographs that the quality of the cut at the beam exit is greatly improved by the control scheme. Ideally, no kerf widening should be observable under the power profiles adopted, but assumptions and simplifications in the model and the ability of the laser to respond to such commands result in some quality deviations.

CONCLUSIONS

A model-based optimisation strategy for improving laser cutting quality of thin plate is presented. It is based on a numerical description of the process, which accounts for the fact that the front can exhibit mobility on approach to a prescribed boundary. It endeavours to manipulate laser beam power in order to stabilise the cutting front temperature right up to such pre-cut sections. This eliminates the need for trial-and-error based experimentation which is currently adopted. First results obtained from the control scheme show significant improvement in quality through reduced kerf widening effects. PMMA burn prints also gave an insight into the power losses experienced in the laser cutting process. It was shown that although transmission and reflection mechanisms are identifiable during reactive gas cutting of steel, reflection losses are minimised at high processing speeds. Actual visualisation of the dynamic front was achieved through high speed photography, and results clearly show that mobility occurs under the effect of a boundary encroachment.

ACKNOWLEDGMENTS

The authors gratefully acknowledge the support given by the Australian Research Council. Valuable discussions and assistance with the experiments given by Mr R. Fowle, Mr A. Harris and Dr A. Black from the School of Mechanical and Manufacturing Engineering, The University of New South Wales, Australia are also duly acknowledged.

REFERENCES

Arata, Y., Maruo, H., Miyamoto, I., Takeuchi, S., (1979), "Dynamic behaviour in laser gas cutting of mild steel", *Trans. JWRI* **8** (2), 15-26.

Biermann, S., and Geiger, M., (1991), "Integration of diagnostics in high power laser systems for optimisation of laser material processing", *Modeling and Simulation of Laser Systems II*, SPIE **1415**, 330-341.

Di Pietro, P., and Yao, Y.L., (1994), "An investigation into characterizing and optimizing laser cutting quality - a review", *Int. J. Mach. Tools Manufact.* **34** (2), 225-243.

Di Pietro, P., and Yao, Y.L., (1995), "A numerical investigation into cutting front mobility in CO_2 laser cutting", *Int. J. Mach. Tools Manufact.*, **35** (5), 673-688.

Geiger, M., Bergmann, H.W., and Nuss, R., (1988), "Laser cutting of steel sheets", *Laser Assisted Processing*, SPIE **1022**, 20-33.

Gonsalves J.N., and Duley, W.W., (1972), "Cutting thin metal sheets with the cw CO_2 laser", *J. Appl. Phys.* **43** (11), 4684-4687.

Miyamoto, I., Maruo, H., and Arata, Y., (1984), "Intensity profile measurements of focussed CO_2 laser beam using PMMA", *ICALEO*, LIA **44**, 313-320.

Miyamoto, I., Maruo, H., and Arata, Y., (1986), "Beam absorption mechanism in laser welding", *Laser Processing: Fundamentals, Applications, and Systems Engineering*, SPIE **668**, 11-18.

Moriyasu, M., Hiramoro, S., Hoshinouchi, s., and Ohmine, M., (1986), "Adaptive control for high-speed and high-quality laser cutting", *Proc. ICALEO'85*, 129-136.

Powell, J., Ivarson, A., Kamalu, J., Broden, G., and Magnusson, C., (1992), "The role of oxygen purity in laser cutting of mild steel", *ICALEO*, SPIE **1990**, 433-442.

Powell, J., (1993a), *CO_2 Laser Cutting*. Springer, London, pp. 218-222.

Powell, J., Ivarson, A., and Magnusson, C., (1993b), "Laser cutting of steels: A physical and chemical analysis of the particles ejected during cutting", *J. Laser Appl.* **5** (1), 25-31.

Schreiner-Mohr, U., Dausinger, F., and Hugel, H., (1991), "New aspects of cutting with CO_2 lasers", *ICALEO*, SPIE **1722**, 263-272.

Yilbas, B.S., et al., (1990), "Study into the measurement and prediction of penetration time during CO_2 laser cutting process", *J. Engng Manufact., Part B*, **204**, 105-113.

Yuan, S.F., Querry, M., and Bedrin, C., (1988), "Thermical modelisation of laser cutting process", *Laser Technologies in Industry*, SPIE **952**, 583-591.

APPENDIX

In the case where an appropriate initial temperature distribution is required prior to cutting, Eqn. (16) calculates the new nodal temperature at time j+1 under the implicit formulation.

Condition: {X = 0 & 0 < (Y=Y_d) <L} & Assist Gas = Oxygen

$$T_{m,n}^{j+1} = \frac{T_{m,n}^{j} + \sigma\left[\frac{H}{KD} + T_{m-1,n}^{j+1} + T_{m+1,n}^{j+1} + 2T_{m,n+1}^{j+1} + Bi_f\frac{T_\infty \Delta y}{D} + Bi_n\frac{T_\infty \Delta y}{D} + 2Bi_r\frac{T_\infty \Delta y}{D}\right]}{\left(1 + 4\sigma + \sigma Bi_f\frac{\Delta y}{D} + \sigma Bi_n\frac{\Delta y}{D} + 2\sigma Bi_r\frac{\Delta y}{D}\right)} \tag{16}$$

where

$$H = P_b(0) + P_{exo} - P_{melt} \tag{17}$$

$$\sigma = \frac{\alpha \Delta t}{\Delta y^2} \tag{18}$$

$$Bi_f = \frac{h_f \Delta y}{K}, \qquad Bi_n = \frac{h_n \Delta y}{K}, \qquad Bi_r = \frac{h_r \Delta y}{K} \tag{19}$$

With cutting underway, the above equation is corrupted to the following form because of the existence of the kerf:

Condition: {X = 0 & 0 < (Y=Y_b) <L} & Assist Gas = Oxygen

$$T_{m,n}^{j+1} = \frac{T_{m,n}^{j} + \sigma\left[\frac{H}{KD} + T_{m+1,n}^{j+1} + 2T_{m,n+1}^{j+1} + Bi_f T_\infty + Bi_f\frac{T_\infty \Delta y}{D} + Bi_n\frac{T_\infty \Delta y}{D} + 2Bi_r\frac{T_\infty \Delta y}{D}\right]}{\left(1 + 3\sigma + \sigma Bi_f + \sigma Bi_f\frac{\Delta y}{D} + 2\sigma Bi_r\frac{\Delta y}{D} + \sigma Bi_n\frac{\Delta y}{D}\right)} \tag{20}$$

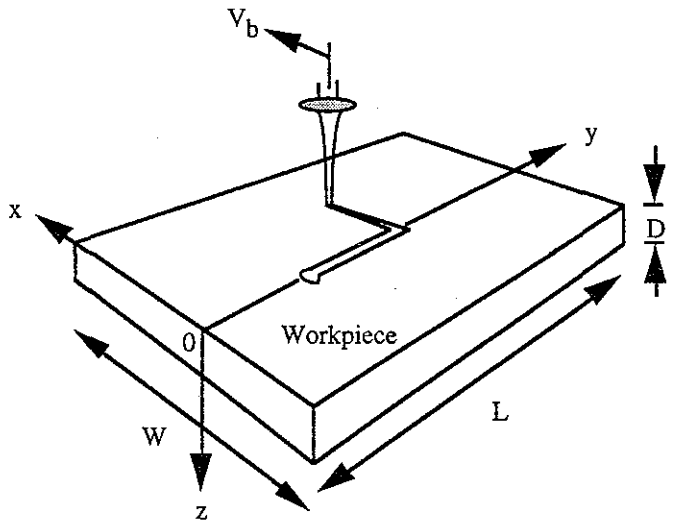

FIG. 1 WORKPIECE CONTROL VOLUME AND BOUNDARIES

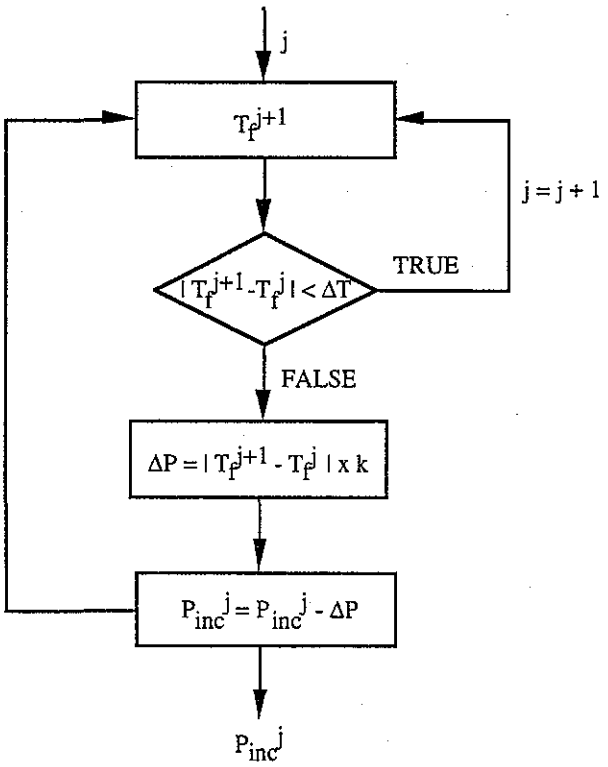

FIG. 2 OPTIMISATION STRATEGY FOR CUTTING FRONT TEMPERATURE STABILISATION

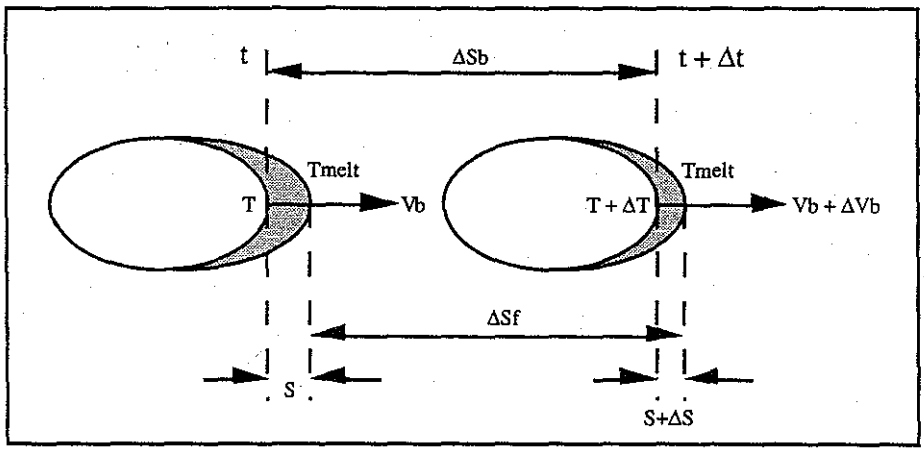

FIG. 3 SCHEMATIC OF CUTTING FRONT MOBILITY OVER A TIME INTERVAL

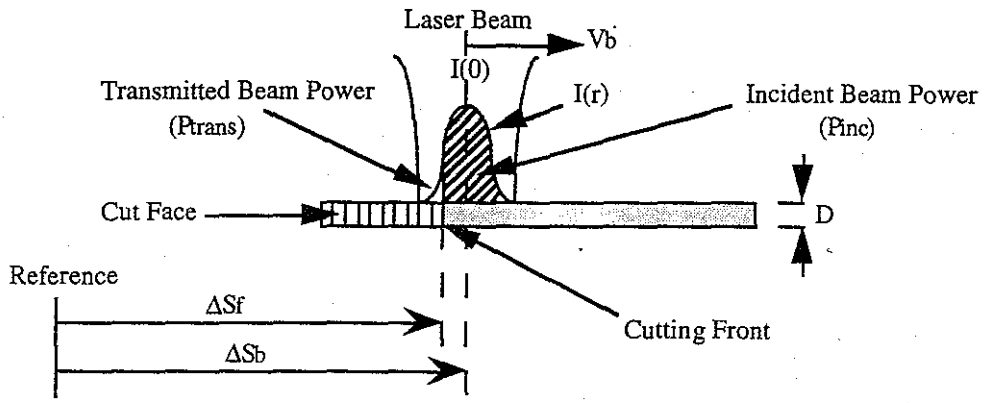

FIG. 4 LASER BEAM ABSORPTION AND TRANSMISSION LOSSES IN LASER CUTTING

TABLE 1 PHYSICAL QUANTITIES AND PARAMETERS USED IN THE NUMERICAL MODEL

Gaussian TEM_{00} CO_2	Assist gas: O_2
5" focal lens	K = 51 W/mK
amu = 71.847 g/mol	T_{melt} = 1809.15 K
R_b = 250 μm	σ_b = 5.67E -8 W/m^2K^4
A_b = 0.4	L_f = 275 kJ/kg
α = 1E -5 m^2/s	ρ = 7865 kg/m^3
ΔH = -257.58 kJ/mol	$\Delta x = \Delta y$ = 250 μm

TABLE 2 SIMULATION AND EXPERIMENTAL CONDITIONS

	500 W	600 W	800 W
10 mm/sec	1	1 & 2	
20 mm/sec	1	1, 2, 3 &4	4
30 mm/sec	1	1, 2 & 4	4
40 mm/sec		2	
60 mm/sec		2	
80 mm/sec		2	
100 mm/sec		2	

1 - thermocouple validation
2 - PMMA burn prints
3 - cine photography
4 - power adaption trials

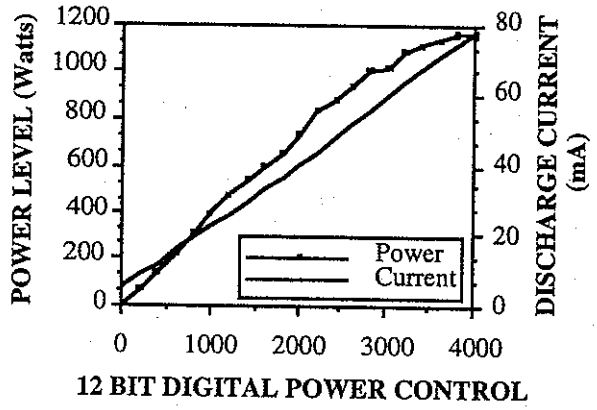

FIG. 5 ACTUAL POWER LEVELS OBTAINABLE AS A FUNCTION OF DISCHARGE CURRENT AND DIGITAL CONTROL WORD (power probe exposure time: 20 sec, gas consumption rate: 150 L/hr)

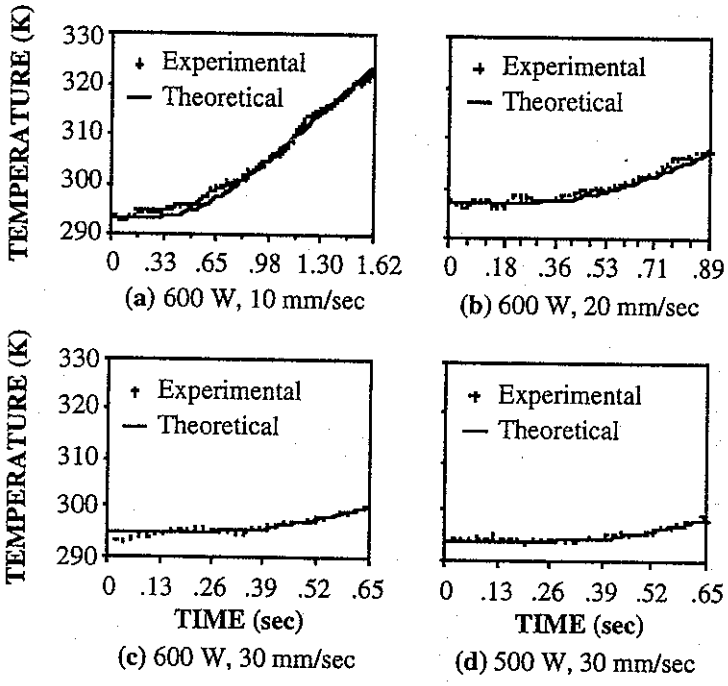

FIG. 6 TYPICAL THERMOCOUPLE TEMPERATURE MEASUREMENTS OBTAINED 2 mm IN FROM THE WORKPIECE CORNER NEAREST THE INITIATION POINT IN BOTH THE X AND Y DIRECTIONS

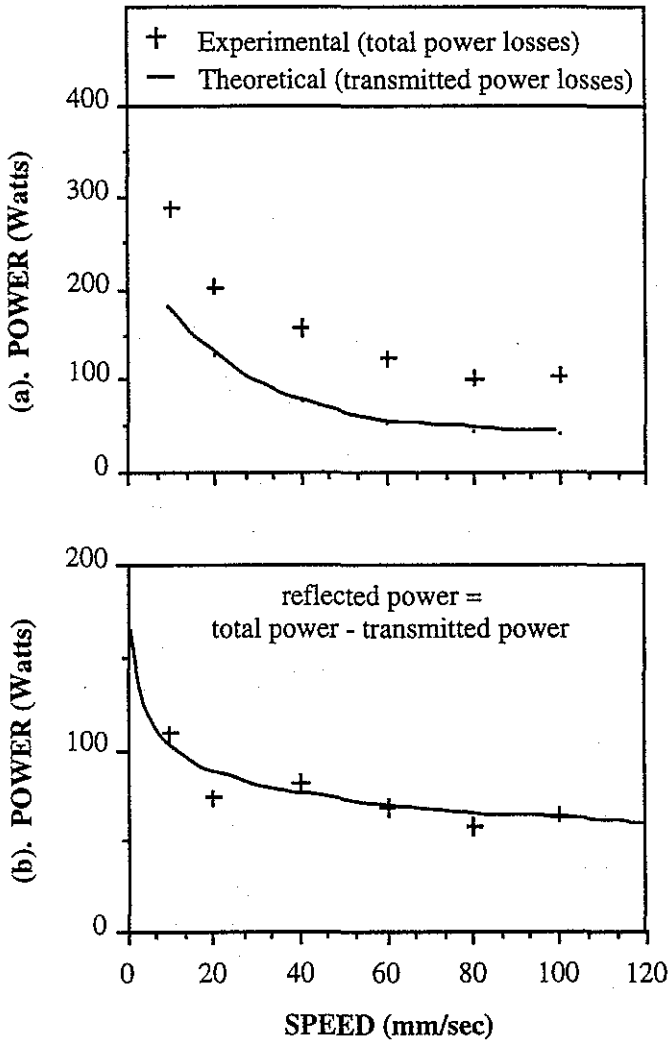

FIG. 7 (a) COMPARING STEADY-STATE TOTAL POWER LOSSES DETERMINED FROM THE PMMA BURN PRINTS WITH TRANSMITTED POWER LEVELS. (b) ESTIMATING STEADY-STATE REFLECTED POWER LOSSES (laser power: 600 W)

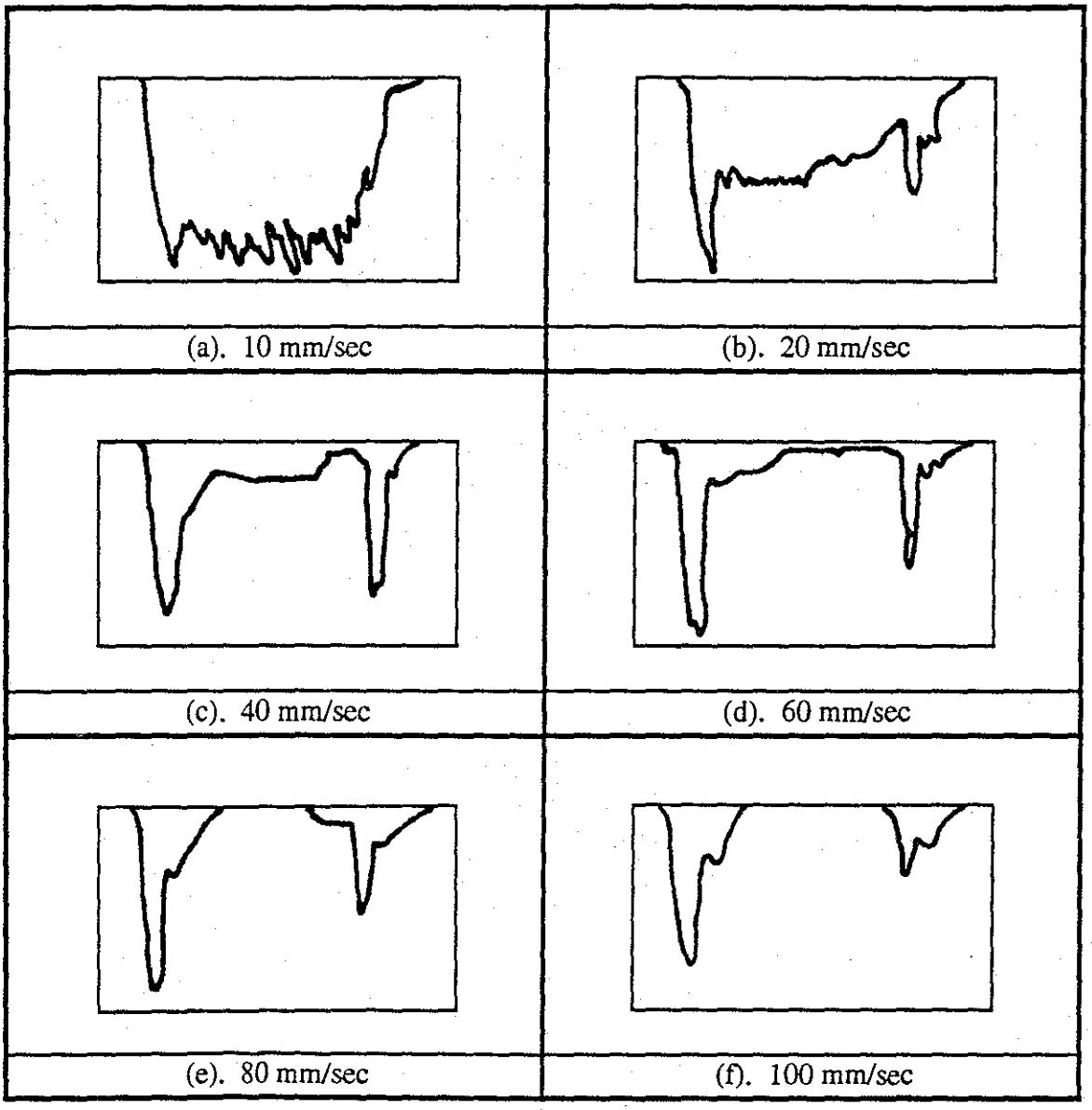

FIG. 8 CROSS-SECTIONAL TRACES OF THE PMMA BURN PRINTS OBTAINED FROM EXPERIMENTS (laser power: 600 W)

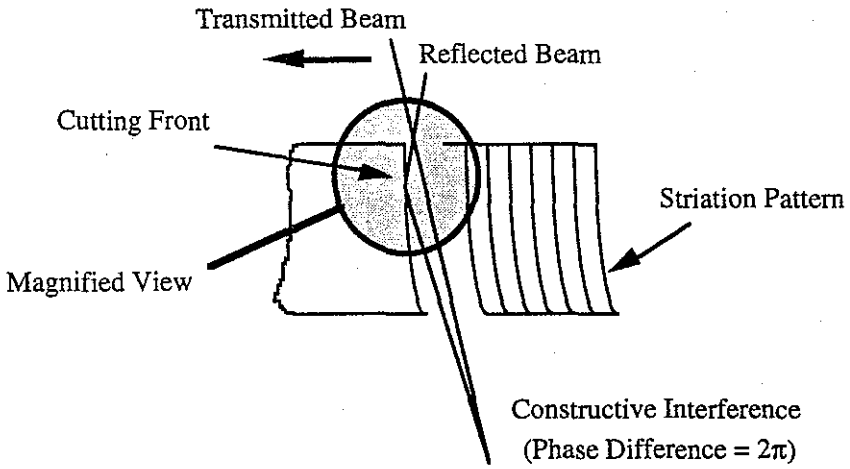

FIG. 9 SCHEMATIC OF THE TRANSMISSION AND REFLECTION MECHANISMS OCCURRING IN THE LASER CUTTING PROCESS

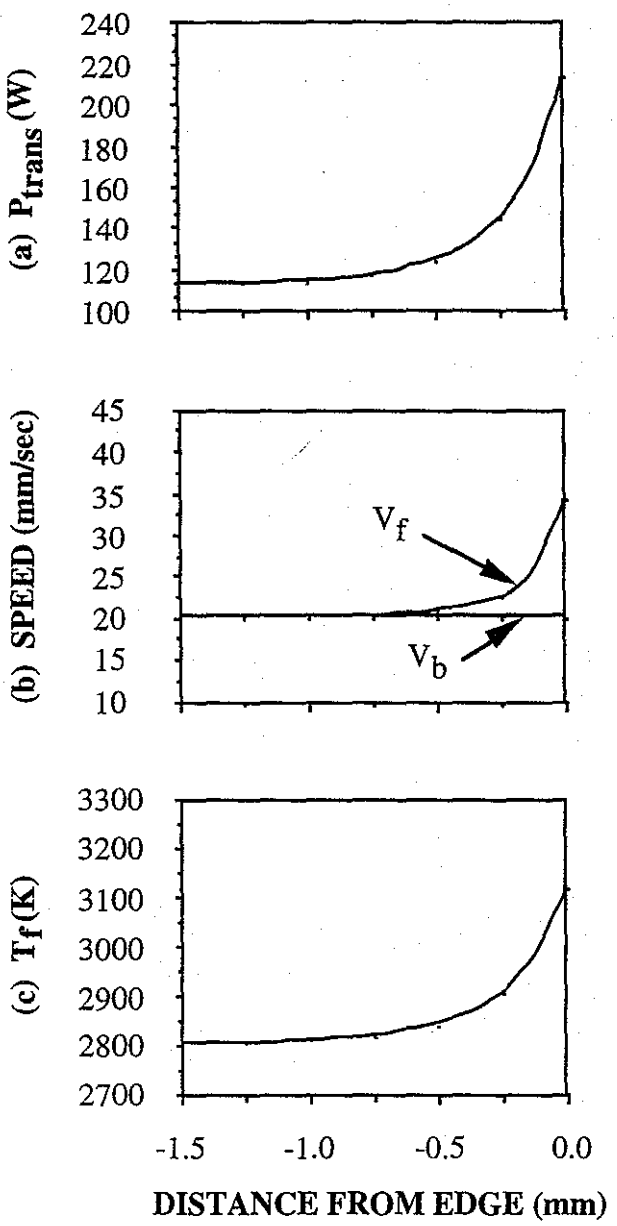

FIG. 10 THE EFFECT OF BOUNDARY ENCROACHMENT ON (a) TRANSMITTED POWER (b) CUTTING FRONT MOBILITY (c) CUTTING FRONT TEMPERATURE (cutting speed: 20 mm/sec, laser power: 600 W)

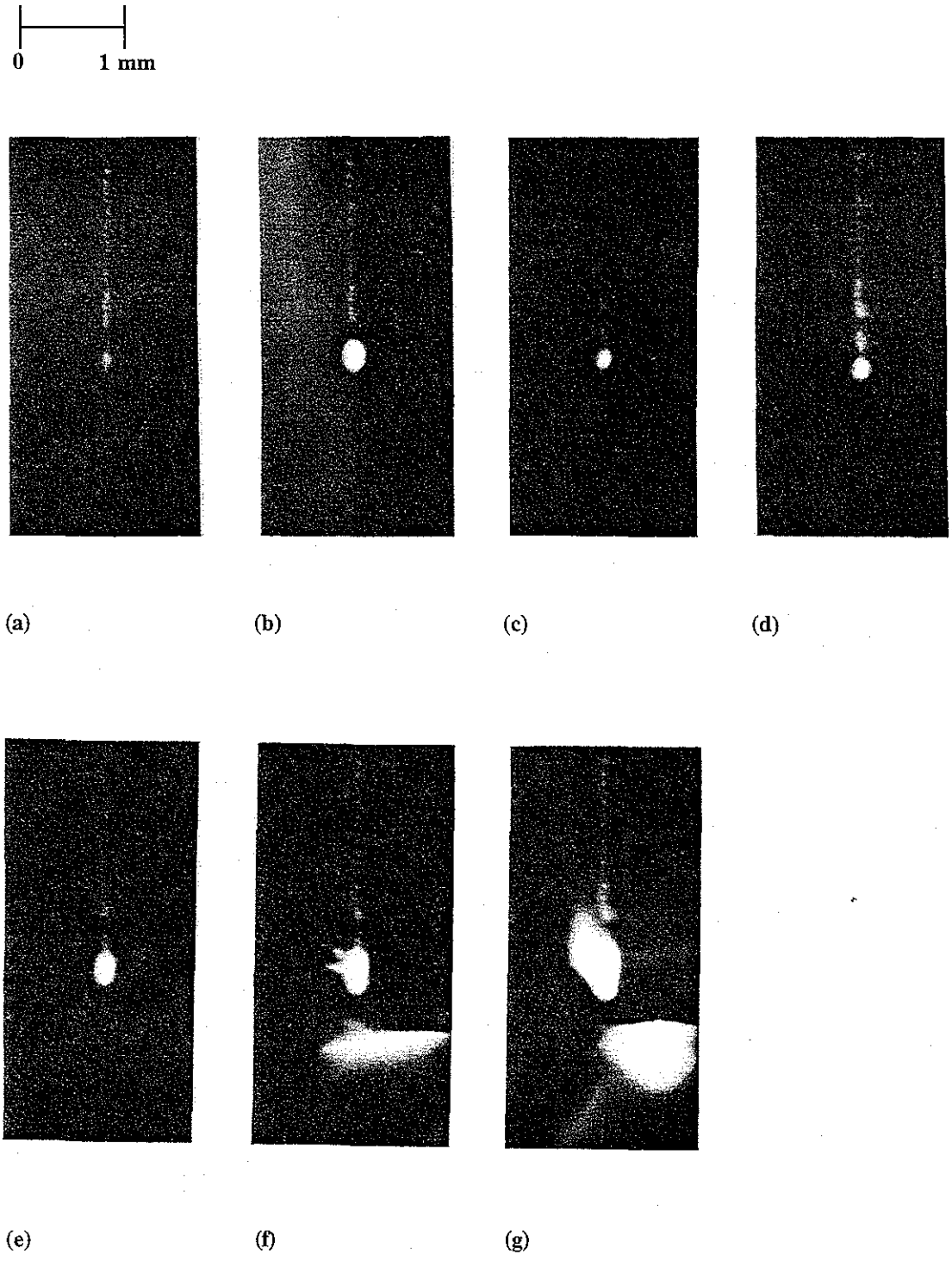

FIG. 11 HIGH SPEED CINE PHOTOGRAPHS TAKEN UNDER BOUNDARY ENCROACHMENT CONDITIONS PERPENDICULAR TO THE CUT AT 15° DECLINATION WITH A FRAME INTERVAL OF 0.002 sec (cutting speed: 20 mm/sec, laser power: 600 W)

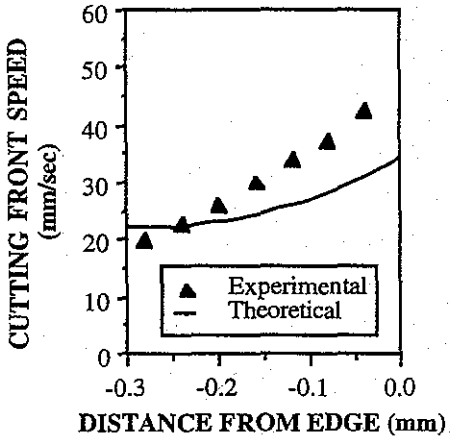

FIG 12 COMPARING THEORETICAL AND EXPERIMENTAL CUTTING FRONT MOBILITY ON APPROACH TO A WORKPIECE BOUNDARY BASED ON VISUALISATION OF THE INTERACTION ZONE (cutting speed: 20 mm/sec, laser power: 600 W)

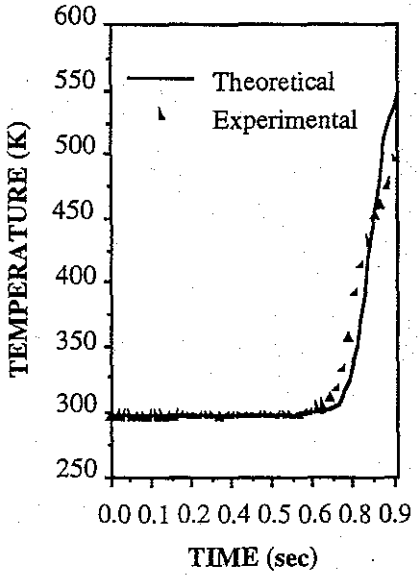

FIG. 13 TYPICAL THERMOCOUPLE TEMPERATURE MEASUREMENT IMBEDED 1.5 mm IN FROM THE BOUNDARY EDGE AND FROM THE LINE OF CUT AS COMPARED TO THE NUMERICAL SOLUTION (cutting speed: 20 mm/sec, laser power: 600 W)

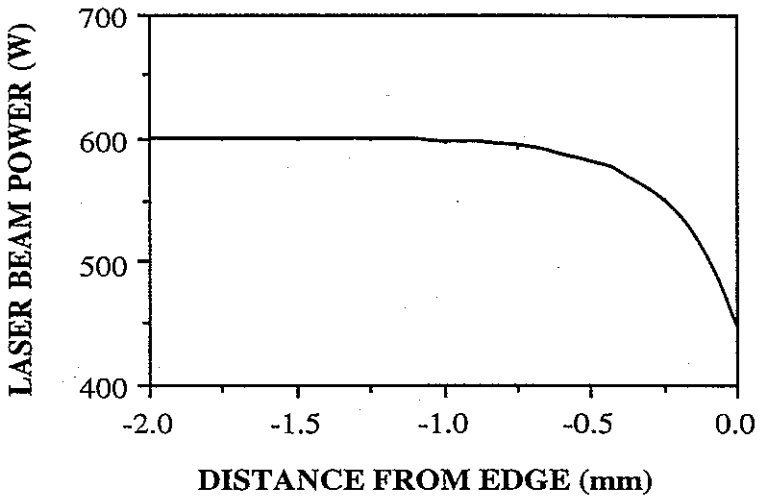

Fig. 14 LASER BEAM POWER PROFILE REQUIRED FOR TEMPERATURE STABILISATION ON BOUNDARY ENCROACHMENT (cutting speed: 20 mm/sec, initial laser power: 600 W)

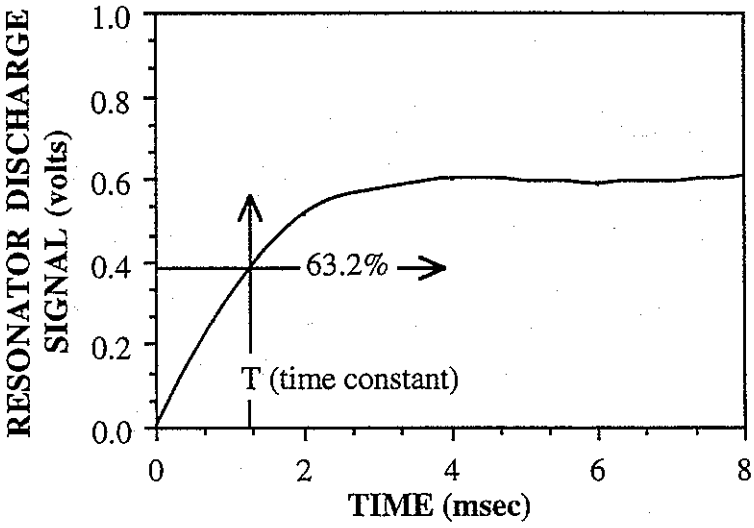

FIG. 15 RESPONSE CURVE OF THE DISCHARGE CURRENT SUBJECTED TO A LARGE STEP INPUT FROM ZERO BEAM POWER TO 1 kW

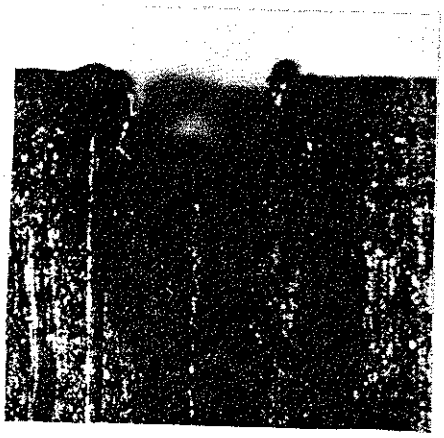

(a) **without power adaption**
(20 mm/sec, 600 W)

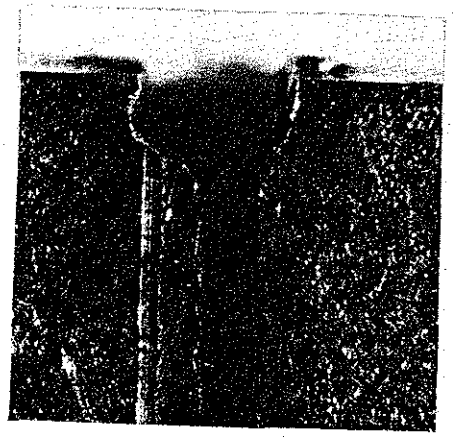

(c) **without power adaption**
(30 mm/sec, 800 W)

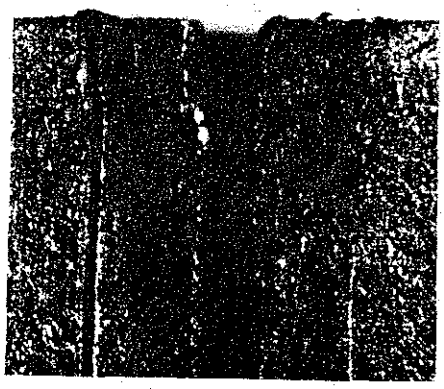

(b) **with power adaption**
(20 mm/sec, 600 W)

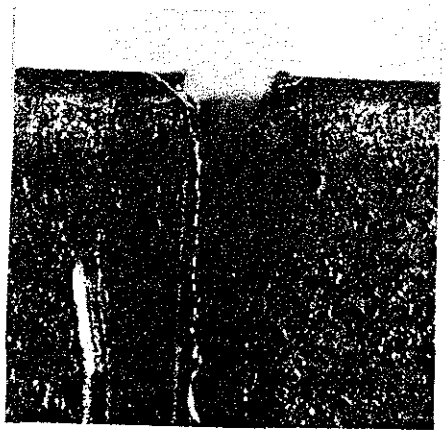

(d) **with power adaption**
(30 mm/sec, 800 W)

FIG. 16 PHOTOGRAPHS COMPARING OBTAINABLE QUALITY WITH AND WITHOUT LASER POWER ADAPTION UNDER DIFFERENT CUTTING CONDITIONS